International Journal of Hydrogen Energy 101 (2025) 731–740

Contents lists available at ScienceDirect

International Journal of Hydrogen Energy

journal homepage: www.elsevier.com/locate/he

Cuprous oxide-*Shewanella* mediated photolytic hydrogen evolution

Michele Morgante [a,d], Nick Vlachopoulos [b], Linfeng Pan [b], Meng Xia [b], Christos Comninellis [c], Kevin Sivula [d], Michael Graetzel [b], Fabian Fischer [a,e,*]

[a] Institute of Life Sciences, HES-SO Valais, University of Applied Sciences Western Switzerland, Rue de l'Industrie, 19, 1950, Sion, Switzerland
[b] Laboratory of Photonics and Interfaces, Institute of Chemical Sciences and Engineering Swiss Federal Institute of Technology in Lausanne (EPFL), Station 6, 1015, Lausanne, Switzerland
[c] School of Chemical Science and Engineering (ISIC), Swiss Federal Institute of Technology in Lausanne (EPFL), Station 6, 1015, Lausanne, Switzerland
[d] Laboratory for Molecular Engineering of Optoelectronic Nanomaterials, Institute of Chemical Sciences and Engineering, Swiss Federal Institute of Technology in Lausanne (EPFL), 1015, Lausanne, Switzerland
[e] Institute of Sustainable Energy, HES-SO Valais, University of Applied Sciences Western Switzerland, Rue de l'Industrie, 23, 1950, Sion, Switzerland

ARTICLE INFO

Keywords:
Microbial fuel cell
Electrogens
Photoelectrode
Semiconductor

ABSTRACT

Hydrogen could be an environmentally friendly option as an energy vector for the future. However, its green production process is expensive, involving water electrolysis, which requires a significant amount of energy. New technologies have been developed to decrease the cost associated with water electrolysis, such as using microbial electrolysis cells (MECs). The integration of power performance enhancing elements into bioelectric systems is of applied interest. As in this work the integration of a photocathode into the microbial electrolysis cell, the energy output increases in theory without needing more reactor space. The microbial electrolysis process requires an additional energy input to overcome the theoretical thermodynamic barrier if any and the involved overpotentials for reasonable rate of hydrogen production. In this work, a microbial electrolysis half-cell was combined with a photoelectrochemical half-cell, so called MPEC (microbial photoelectrochemical cell). The MPEC consisted of a *Shewanella oneidensis* MR-1 bioanode and a five-layered p-type Cu_2O-based photocathode, using lactate as electron donor to produce H_2 without any external bias than light of 210 and 700 W m^{-2}.

The novelty of the work can be summarized in the following points: The use of MPEC for H_2 production with a stable and efficient multilayer Cu_2O photocathode. The quantification of the anodic, cathodic and global coulombic efficiencies considering the selectivity of lactate to acetate conversion. The electrochemical characterization (I–V curves) of the bioanode and photocathode for the determination of the electrode which limit the current in the process. Proposition of a model to explain the low anodic coulombic efficiencies (7 ± 2%). In this model lactate may be involved in either a surface reaction at the bioanode (the main reaction producing current) or a bulk aerobic or anaerobic reaction catalysed by planktonic cells (a side reaction that consumes lactate without producing current). This work is of interest of research that aims to integrate multiple processes into bioelectric systems and to use light energy in a direct manner to generate energy vectors such as hydrogen.

1. Introduction

In 2023, the world's population reached 8 billion causing the ever-increasing energy need [1]. The current energy vectors originate from fossil oil refining, whereas this is a finite resource and a major source for CO_2 emissions [2]. To reduce the reliance on fossil fuels, innovative renewable technologies are being developed to generate carbon free fuels [3,4]. This work investigates the generation of one of these carbon-free or neutral energy vectors by using a bioelectric electrolysis cell and solar cell technology.

Hydrogen is readily producible with microbial electrolysis cells (MECs) [5,6]. It is a versatile energy vector and a chemical compound with a higher specific energy content (120 MJ kg^{-1}) compared to the more commonly used methane (44 MJ kg^{-1}). When produced economically from water by electrolysis with renewable electricity such as solar, wind, hydropower, and others, it has the potential to become a major e-fuel. However, current sustainable electrolysis approaches remain expensive [7]. Therefore, researchers have attempted to enhance

* Corresponding author. Institute of Life Sciences, HES-SO Valais, University of Applied Sciences Western Switzerland, Rue de l'Industrie, 19, 1950, Sion, Switzerland.
E-mail address: fabian.fischer@hevs.ch (F. Fischer).

https://doi.org/10.1016/j.ijhydene.2024.12.407
Received 12 March 2024; Received in revised form 11 September 2024; Accepted 23 December 2024

the process and make it more economically competitive [8], as production from natural gas and oil reforming currently dominates [9]. Developing new, economic, and sustainable hydrogen production technologies is a current challenge [10,11].

MECs utilise electrogenic microbes in the anode to bio-catalyse the oxidation of organic matter at a lower anodic potential than that needed for water oxidation to oxygen, in water electrolysis for hydrogen generation. This results in a lower energy input requirement. Commonly used electrogenic microbes include *Shewanella, Geobacter, Aeromonas*, *Rhodopseudomonas* and *Dysgonomonas* [12]. Inoculates from natural ecosystems and wastewater treatment plants can also be utilized to develop electrogenic microbial biofilms [13]. Carbon-based materials, such as carbon felt, graphite and reticulated vitreous carbon (RVC) are preferred electrodes for microbial attachments due to their biocompatibility [14].

The MEC offers an eco-friendly approach for generating hydrogen. However, its analysis indicates that the process requires supplementary energy input to overcome the thermodynamic barrier (if any) of involved overpotentials (both cathodic and anodic) and cell resistance, in order to achieve a reasonable rate of hydrogen production [15]. Solar energy has recently been proposed as a feasible alternative to produce this additional energy [16]. Two main systems have been employed: the ex-cell and in-cell systems [17,18].

The ex-cell solar configuration utilizes an external photovoltaic device (e.g. a dye-sensitized solar cell) [16], while an in-cell semiconductor electrode (p-Cu_2O, n-TiO_2 or n-WO_3) functions as the photocathode [19–21]. This configuration has been reported as a microbial photoelectrochemical cell (MPEC) [17].

The successful use of TiO_2 as a photocathode for hydrogen evolution using the MPEC configuration without external voltage application has been reported [20,22]. However, due to its large band gap, E_g of 3.2 eV, TiO_2 is only photoactive under UV light, which accounts for only 4% of terrestrial solar energy. In contrast, a WO_3 ($E_g = 2.7$ eV) photocathode has also been used in the microbial photoelectrochemical cell to produce hydrogen under both visible light irradiation and external bias application [21]. However, both TiO_2 and WO_3 are typically n-type semiconductors and are not optimally suited to perform as photocathodes.

Another potential material is the p-type polyaniline nanofiber. The material generates photoelectrons when exposed to fluorescent light, which reduces protons to hydrogen in a single chamber MEC [23]. Hydrogen can also be produced in a non-membrane MPEC using a $ZnFe_2O_4$/g-C_3N_4 photocathode [24].

However, the MPEC process has recently garnered attention due to the development of the cuprous oxide (Cu_2O) p-type photocathode [25]. This photocathode has a bandgap of approximately 2 eV, making it responsive to visible light with a theoretical photocurrent of −14.7 mA cm^{-2} under standard 1-Sun illumination [26].

The primary issue with using Cu_2O as a photocathode for hydrogen evolution is its instability in aqueous solutions. Its reduction potentials [+0.3 to +0.45 V versus the reversible hydrogen electrode, (RHE)] are lower (more positive) than the hydrogen evolution potential. This makes the reduction of Cu_2O to metallic Cu at the Cu_2O/electrolyte interface (Eq. (1)) more favourable compared to water reduction to hydrogen.

$$Cu_2O + H_2O + 2e^- \rightarrow 2Cu + 2OH^- \quad (1)$$

Several research groups have made efforts to improve the photoelectrochemical performance of Cu_2O-based photocathodes. This has been achieved by introducing charge extraction under a protective overlayer, as well as various hydrogen evolution electrocatalysts. These findings were discussed in a recent review paper [27]. Liang et al. [19] have reported the deposition of a NiO_x layer on Cu_2O (Cu_2O/NiO_x) to enhance its stability. That study found that the addition of a NiO_x layer to Cu_2O photocathode had a trade-off effect on the performance. Specifically, increasing the thickness of the NiO_x film on Cu_2O resulted in a decrease in photocurrent, but an increase in stability of the Cu_2O electrode. The optimal thickness for the NiO_x layer was found to be 240 nm, which allowed the Cu_2O/NiO_x composite photocathode to produce H_2 solely upon an external bias application (0.2 V) under solar irradiation [19]. No significant hydrogen production was observed under open circuit conditions.

Table 1
Comparison of hydrogen production with dual chambered microbial electrolysis cells in the literature. a) Simulated solar light. b) Cathode surface. c) Calculated per cm^{-2} from reported data. The absolute hydrogen rate production could differ in different devices (e.g. internal resistance, bioanode activity).

Photocathode	External bias	Microbial Anode [inoculum]	H_2 rate [μL h^{-1} cm^{-2}][b]	References
n-TiO_2	300 W Xenon lamp (solar simulator)	Anaerobic sludge	2.20[c]	Chen et al. (2013) [20]
n-TiO_2	30 W low-pressure mercury lamp	Anaerobic sludge	0.14[c]	He et al. (2014) [22]
p-Cu_2O/NiO_x	Light and power supply 0.2 V	Anaerobic sludge	5.09	Liang et al. (2016) [19]
n-WO_3	Light and external power supply 0.3 V	Anaerobic sludge	10.67	Tahir (2019) [21]

In other work the photoelectrode was coated with MoS_2 as a catalyst for hydrogen evolution, representing a low-cost alternative to expensive Pt and similar solutions. The corresponding MPEC readily produced hydrogen with an external bias of −0.8 V and simultaneous light irradiation [28].

The research of Liang et al. (2016) [19] was based on a similar photoelectrode (Table 1). The low applied voltage of 0.2 V was just above the theoretical needed value of 0.13 V (using acetate as electron donor). This explained the comparatively low productivity with 5.09 μL h^{-1} cm^{-2} of hydrogen. Table 1 presents results obtained using anaerobic sludge, where the anodic and overall coulombic efficiency remained unquantified. As a result, only the cathodic coulombic efficiency was reported.

The schematic representation of the microbial photoelectrochemical cell (MPEC) system used in this study is shown in Fig. 1 which demonstrates that photogenerated electrons at the Cu_2O-based photocathode conduction band (CB) reduce water to hydrogen (Eq. (2)). Meanwhile, the electrons generated by lactate ($C_3H_5O_3^-$) oxidation on the *S. oneidensis* MR-1 bioanode, to acetate (Eq. (3)) or/and bicarbonate (Eq. (4)), are transferred through the external circuit to the valence band of the photocathode where they recombine with holes. To maintain charge electroneutrality, cations are transferred from the anolyte to the catholyte through the Nafion® membrane.

$$4H_2O + 4\,e^- \rightarrow 2H_2 + 4\,OH^- \quad (2)$$

$$C_3H_5O_3^- + 2H_2O \rightarrow CH_3COO^- + HCO_3^- + 5H^+ + 4e^- \quad (3)$$

$$C_3H_5O_3^- + 6H_2O \rightarrow 3HCO_3^- + 14H^+ + 12e^- \quad (4)$$

The global reaction indicates that 2 mol of hydrogen are produced per mole of lactate consumed when considering Eq. (3) as the anodic reaction (Eq. (5)) and 6 mol of hydrogen per mole of lactate consumed when considering Eq. (4) as the anodic reaction (Eq. (6)):

$$C_3H_5O_3^- + 2H_2O \rightarrow CH_3COO^- + HCO_3^- + H^+ + 2H_2 \quad (5)$$

$$C_3H_5O_3^- + 6H_2O \rightarrow 3HCO_3^- + 2H^+ + 6H_2 \quad (6)$$

Equations (5) and (6) are associated with 4 and 12 electrons in their respective anodic half-reactions.

The photocathode and bioanode operate together to combine the solar energy with the bio-catalysis-related chemical energy of lactate, resulting in the production of hydrogen (Eqs. (5) and (6)).

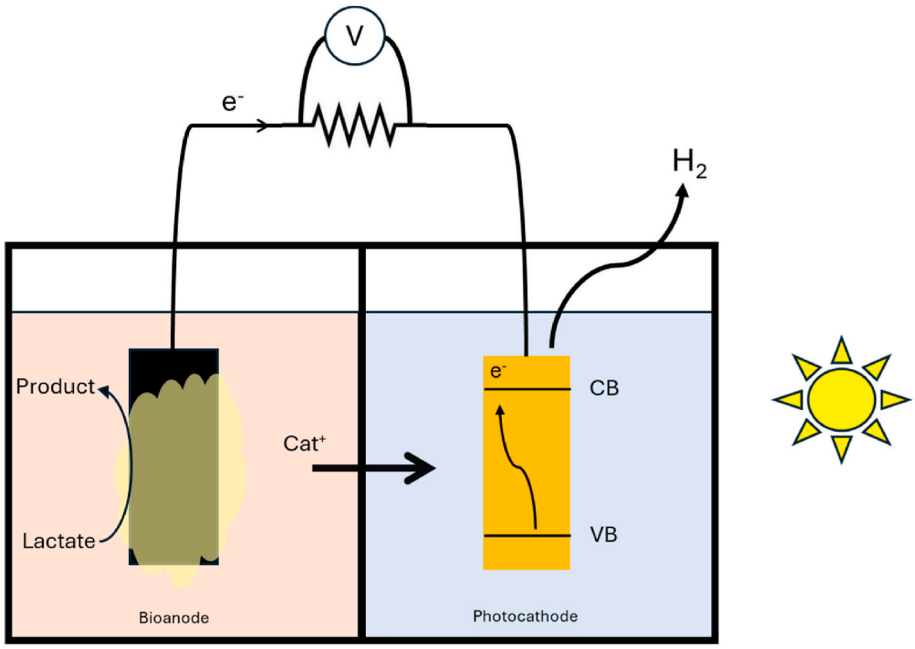

Fig. 1. Schematic presentation of the microbial photoelectrochemical cell (MPEC) with S. oneidensis MR-1 bioanode and Cu_2O based photocathode for hydrogen evolution. The generated electrons at the bioanode, by lactate oxidation (Eqs. (3) and (4)), recombine with the holes in the valence band (VB) of the Cu_2O photocathode, while the photogenerated electrons in the conduction band (CB) reduce water to hydrogen (Eq. (2)). To respect electroneutrality, cations (Cat^+) are transferred from the anolyte to the catholyte through the Nafion® membrane.

The main side reaction in the anolyte, which can consume lactate without producing current, is the fermentation of lactate to acetate and hydrogen (Eq. (5) stated above). This reaction is catalysed by planktonic *Shewanella* cells [29].

From a thermodynamic perspective, the reaction is exergonic ($\Delta G = -4.2\ kJ\ mol^{-1}$) under standard conditions at pH = 7 with $E^{0'} = +0.011$ V vs the standard hydrogen electrode (SHE) [30]. A recent publication [31] demonstrated that eliminating *hydA* and *hyaB* hydrogenase in *Shewanella* resulted in higher current density and coulombic efficiency by redirecting electron flow towards the anode, rather than lactate fermentation (Eq. (5)) in the anolyte.

Finally, the selectivity of lactate to acetate transformation (S) was defined as the ratio between the amount of formed acetate (n_{Acet}^{form}) and the amount of consumed lactate (n_{Lact}^{cons}) after a given time t of electrolysis (Eq. (7)).

$$S = \frac{n_{Acet}^{form}}{n_{Lact}^{cons}} \tag{7}$$

For the first time, in this work, hydrogen shall be produced using a microbial photoelectrochemical cell (MPEC) with a stable and efficient photocatalytic multilayer Cu_2O photocathode. The photocathode was deposited on a fluorine-doped tin oxide (FTO) substrate ($Au/Cu_2O/Ga_2O_3/TiO_2/RuO_x$) and it was attempted to use no external bias to produce H_2 in the MPEC. The dark bioanode was acclimatized with *Shewanella oneidensis* MR-1 in a two-compartment cell, using lactate as an electron donor, and a Nafion® membrane. The experiment measured the photocurrent production, lactate consumption, acetate production in the anodic compartment, and hydrogen evolution in the cathodic compartment. From these measurements, several crucial values will be derived, including the selectivity of lactate to acetate transformation in the anolyte (S) and the cathodic coulombic efficiency for H_2 production based on the electrical charge passed Q $\left(CCE_{H_2}^{Q}\right)$. The anodic coulombic efficiency based on the conversion of lactate to the reaction products at the bioanode $\left(ACE_{\text{prod.}}^{Lact}\right)$ and the overall coulombic efficiency based on the conversion of oxidized lactate at the bioanode to the produced H_2 at the photocathode $\left(OCE_{H_2}^{Lact}\right)$ were intended to be determined for an MPEC mediated hydrogen production. This is the first time that all these parameters will be determined. The bioanode and photocathode were electrochemically characterised, to identify which electrode is limiting the current in the process.

Finally, a model is to be proposed to explain the low anodic coulombic efficiency.

2. Materials and methods

2.1. Low-scan linear voltammetry of photocathode

A three-electrodes photoelectrochemical (PEC) cell was used, with the Cu_2O-based photocathode (0.5 cm^2) as the working electrode, a platinum electrode as the counter electrode (6.25 cm^2, PT542502, 25 × 25 mm, Advent Research Materials, UK), and Ag/AgCl sat KCl (Biologic, France) as the reference electrode. The electrolyte used was 0.1 M phosphate buffer solution at pH 7. The photocathode was exposed to one-sun simulated irradiation using a 300 W xenon lamp. For more details, refer to Pan et al., 2018 [32].

2.2. Low scan linear voltammetry of bioanode

Low-scan linear voltammetry was performed on the acclimatized bioanode using a single-compartment cell with a three-electrode system. The working electrode (WE) was a graphite rod (7.54 cm^2), the counter electrode (CE) was a platinum mesh (6.25 cm^2), and the reference electrode (RE) was an Ag/AgCl sat. KCl (0.197 V vs. the standard hydrogen electrode at 25 °C). The experiments were conducted at a constant temperature (25 °C) using the minimal medium (MM) [33] as electrolyte. Prior to recording measurements, the medium was purged with nitrogen (5.0 quality) and left unstirred. The working electrode was maintained at the open circuit potential (OCP) for 5 min before each measurement.

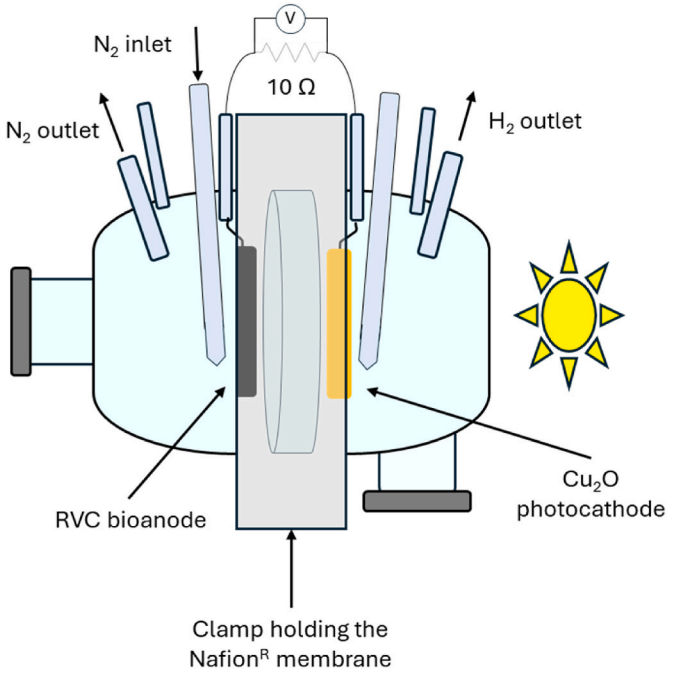

Fig. 2. Schematic representation of the microbial photoelectrochemical cell (MPEC) with *S. oneidensis* MR-1 bioanode and light-irradiated photocathode for hydrogen evolution. $V_{anolyte}$ = 25 mL, S_{anode} = 12 cm^2, $V_{catholyte}$ = 40 mL, $S_{cathode}$ = 0.5 cm^2, RVC: reticulated vitreous carbon. The used bioanode surface area was much larger than that of the photocathode because the expected photocurrent at the cathode was much higher than the bio-current to the anode.

2.3. Microbial-photoelectrochemical cell for H_2 production

Fig. 2 presents a schematic presentation of the two compartments of the MPEC cell in borosilicate glass (manufactured by a glassblower, Cardis, Monthey, Switzerland). The borosilicate glass reactor was sterilized at 121 °C for 21 min before use.

The anodic compartment was filled with 25 mL of medium (20 mM lactate in 5 g L^{-1} NaCl, 2.5 g L^{-1} K_2HPO_4, 17 g L^{-1} tryptone, 3 g L^{-1} soytone). The cathodic compartment (cathode surface area of 0.5 cm^2) was filled with 40 mL of catholyte, which was a 0.1 M phosphate buffer (pH 7). The two compartments were separated by a Nafion® 117 proton-exchange membrane (Ion Power, New Castle, USA). The anode and cathode electrodes were positioned 0.5 cm away from the membrane.

The anode compartment was fitted with a gas inlet tip to allow for N_2 bubbling (5.0 quality) at a flow rate of 20 mL min^{-1}. A PFTE filter with a porosity of 0.45 μm (HPLC quality) was used. The anode was a disk-shaped electrode made of reticulated vitreous carbon (Fig. 3c) with a surface area of 12 cm^2 and a pore size of 100 ppi (RVC, *ERG aerospace corporation*, USA). The electrode was connected to an insulated copper wire using silver-doped epoxy glue (8331-14G MG Chemicals, United Kingdom). The glued electrode was dried at 65 °C on a hot plate for 15 min. To ensure that the resistance between the connecting copper wire and the electrode was less than 15 Ω, a voltmeter (Voltcraft PLUS VC960) was used to control it. The surface of the connecting conductive glue surface was covered with an insulating glue (Loctite HY 4090, United Kingdom). The bioanode was acclimatized according to the method described in Section 2.4.

The cathodic compartment was equipped with a quartz window (2 mm thickness, 35 mm diameter, Cardis, Monthey, Switzerland), a gas collection neck with a septum, and two openings for photocathode wiring. The multilayer cuprous oxide (Cu_2O) photocathode was prepared following the procedure described in Section 2.5. At both light intensities, the MPEC was maintained at 25 °C using a magnetic stirrer. The solar light simulator (Solar Simulator, HAL-320, Asahi Spectra Co., Ltd., Japan) was positioned 37 cm away from the setup (recommended by Asahi Spectra), to irradiate the setup with specific intensities for which a calibration was performed.

2.4. Bioanode acclimatization

A two-compartment cell operating as a microbial biofuel cell (MFC)

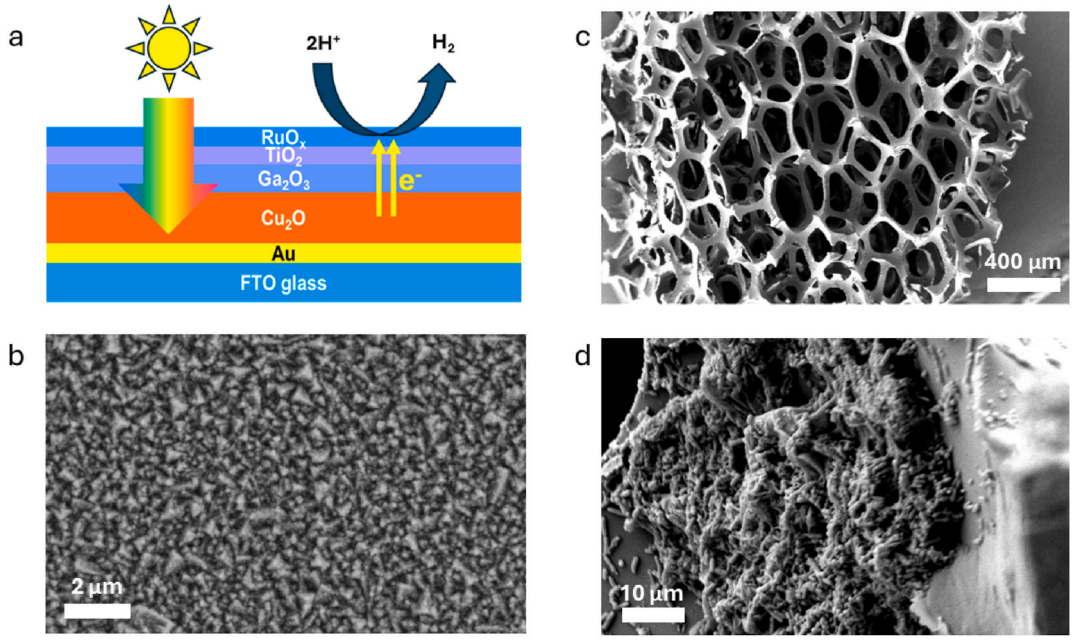

Fig. 3. (a) Schematic photolytic hydrogen evolution mechanism and representation of the multilayer semiconductor Cu_2O based photocathode Au/p-Cu_2O/Ga_2O_3/TiO_2/RuO_x (Cu_2O-GTR) deposited on fluorine-doped tin oxide (FTO) glass substrate. Gold was sputtered (100 nm), Cu_2O was electrodeposited (500–1500 nm), Ga_2O_3 (20 nm) and TiO_2 (20 nm) were deposited by atomic layer deposition (ALD). RuO_x (40 nm) was galvanostatically electrodeposited. SEM images of (b) the multilayer semiconductor photocathode, (c) an RVC electrode without biofilm, and the same (d) with a *S. oneidensis* MR-1 biofilm. (For interpretation of the references to colour in this figure legend, the reader is referred to the Web version of this article.)

was used for acclimatization at the bioanode. The anolyte consisted of a pre-cultivation medium containing 10 g L^{-1} tryptone and 5 g L^{-1} yeast extract (Sigma-Aldrich both, Switzerland) and 10 g L^{-1} NaCl (Luria-Bertani medium) with suspended *S. oneidensis* MR-1 (wild-type strain; ATCC 700550). The catholyte consisted of 50 mM potassium ferricyanide (Thermo Scientific, India) in 0.1 M potassium phosphate buffer (pH 7). The two compartments were separated by a Nafion® membrane. The anode and cathode were connected through an external resistance of 1 kΩ (Resistance Box Voltcraft R-Box 19). During biofilm acclimatization (20 days), the medium in the anode and cathode compartments was replenished when the current decreased [34]. Polarization experiments were conducted to evaluate cell performance.

For the subsequent hydrogen evolution experiments, the RVC electrode containing the mature biofilm (Fig. 3d) was transferred in a laminar flow from an MFC to the slightly different MPEC reactor.

2.5. Photocathode preparation

The photocathode, which was based on cuprous oxide, was composed of a multilayer coating on an FTO (fluorine-doped tin oxide) glass plate. The coating included an Au back contact layer that acted as an ohmic contact, a Ga_2O_3 overlayer facilitated the electron transport towards the surface of the electrode, a TiO_2 protective layer prevented photo-corrosion (Eq. (1)), and a RuO_x catalyst for hydrogen evolution [32].

The Cu_2O/Ga_2O_3 produced a photocurrent of 6.5 mA cm^{-2} in the PEC device [32]. The presence of a protecting layer above the Cu_2O film influenced the constant generation of this photo current positively, as Cu_2O is inherently unstable and was equally found unstable under linear-sweep voltammetry conditions in prolonged use. The used Ga_2O_3 layer generated a dark current, indicating stability issues also from this protecting layer. This dark current was eliminated by coating the Ga_2O_3 surface with a TiO_2 layer. Fig. 3a shows a scheme of this layered photocathode and a SEM picture (Fig. 3b) with a view the top layer. The five layered photo cathode was therefore an Au/p-Cu_2O/Ga_2O_3/-TiO_2/RuO_x (Cu_2O-GTR) photocathode deposited on polished FTO glass support.

For the preparation of the photocathode, a FTO glass plate of 6.6 cm^2 area (TEC-15, G2E-Company, Switzerland) was cleaned by sequential compressed air purging, treated with a 2% aqueous surfactant solution (Hellmanex III, Sigma-Aldrich, Switzerland), and sonicated (VWR, Ultrasonic cleaner, 35 kHz) for 30 min. Finally, it was dried using compressed air.

The gold back contact layer (3.2 μm) was deposited using an Alliance Concept DP650 device at a 2.65 nm s^{-1} growth rate for 20 min in a clean room. Subsequently, the Cu_2O layer was electrodeposited using a buffered solution prepared from 7.98 g of $CuSO_4$ (Sigma-Aldrich, Switzerland), 67.5 g of lactic acid, and 21.77 g of K_2HPO_4 in 250 mL of deionized water. The pH was adjusted to 12 with 2 M KOH [32], and a cathodic current of 0.1 mA cm^{-2} was applied for 100 min/32 °C. (resulting in a thickness between 500 and 1500 nm). Subsequently, two additional overlayers were deposited using thermal atomic layer deposition (Savannah 100, Cambridge NanoTech), for 7 h per layer [32]. Bis-(μ-dimethylamino)-tetrakis-(dimethylamino)-digallium (98%, STREM Chemicals, USA) has been used as precursor for gallium oxide (Ga_2O_3) deposition and tetrakis-(dimethylamino)-titanium (99.999%, Sigma-Aldrich, USA) was the used precursor for titanium dioxide (TiO_2) deposition (resulting in a Ga_2O_3 and TiO_2 thickness of approximately 20 nm). The photoelectrodes prepared as described above were cut into pieces of 0.5 cm^2 area. A layer of RuO_x (electrocatalyst for hydrogen evolution) was then photoelectrochemically deposited onto the electrodes using a 1.3 mM $KRuO_4$ (Sigma-Aldrich, USA) solution in demineralized water (Milli-Q^R), obtaining a thickness of 40 nm. The PEC cell was filled with this solution, with the photoelectrode serving as the working electrode and a Pt wire as the counter electrode. The deposition was carried out with a constant cathodic current (−28 μA cm^{-2}) and simulated one-sun illumination for 6 min [32]. The sheet surface resistance of 15 Ω-square was low enough to generate a uniform electrodeposited film. To delimit exposed surface, epoxy glue (Epoxy adhesive EA 9461 Loctite, *Henkel,* United Kingdom) was used, with subsequent drying on a heating plate 75 °C/5 min. A new photocathode was utilized for each test, to exclude photostability issues. Photo-corrosion and solute deposition where possible with prolonged use.

2.6. Analysis of reactants and products by high performance liquid chromatography

Anolyte samples were analysed by high-performance liquid chromatography (HPLC) to quantify lactate and acetate concentrations during electrolysis. Samples of 1 mL were transferred to a 1.5 mL Eppendorf tube and centrifuged at 4500 rpm for 10 min. An aliquot of the supernatant (10 μL) was injected in the HPLC apparatus (HP series 1100). Sulfuric acid 25 mM prepared from highly concentrated H_2SO_4 99.5% (Thermo Scientific, Germany) and used as mobile phase and by isocratic conditions eluted with 0.6 mL min^{-1}. A Nucleogel Sugar 810 H (Machery-Nagel) column was employed, maintained at 55 °C. It was connected to a refractive index detector (RI, Agilent Technologies 1260 Infinity II, series G7162A). Peaks were integrated by OpenLab^R Data Management software.

2.7. Hydrogen quantification

The photogenerated hydrogen was collected from the cathode's headspace (V = 20 mL) through a silicone cap on top of a gas collection tube with a 2.5 mL gas tight syringe (Hamilton 1002 LT) and injected into a micro-gas chromatography (490 Micro GC, Agilent). The obtained hydrogen concentration was calculated by applying the ideal gas law under standard ambient temperature conditions (SATP, 1 bar and 298.15 K).

2.8. Coulombic efficiencies of the involved transformations

In this work, three main coulombic efficiencies are defined: the cathodic coulombic efficiency, which is related to hydrogen production at the biocathode (Eq. (2)); the anodic coulombic efficiency, which is related to both the partial conversion of lactate to both acetate and bicarbonate and the complete conversion of lactate to bicarbonate only (Eqs. (3) and (4), respectively); and the global efficiency, which is related to the electrochemical generation of hydrogen from lactate (Eqs. (5) and (6)). Mole quantities of lactate and acetate were determined by HPLC analysis in view of actual volumes present in the MPEC at the moment of sampling.

2.8.1. Cathodic coulombic efficiency

The cathodic coulombic efficiency ($CCE^Q_{H_2}$) for H_2 production, expressed as the electrical charge passed *Q*, is the ratio between the experimentally measured of H_2 ($n^{exp}_{H_2}$) and the theoretical quantity calculated using the Faraday's law ($n^{theor}_{H_2}$) based on the electrical charge passed after a given time t of electrolysis (Eqs. (8) and (9)).

$$CCE^Q_{H_2} = \frac{n^{exp}_{H_2}}{n^{theor}_{H_2}} \tag{8}$$

$$n^{theor}_{H_2} = \frac{\int_0^t I\,dt}{2F} \tag{9}$$

2.8.2. Anodic coulombic efficiency

To determine the anodic coulombic efficiency (ACE^{Lact}_{prod}), Eq. (3), Eq. (4) and the selectivity of lactate to acetate conversion (Eq. (7)) were considered. ACE^{Lact}_{prod} represents the ratio of the measured electrical charge passed after a given time t of electrolysis. $\int_0^t I\,dt$ to the theoretical

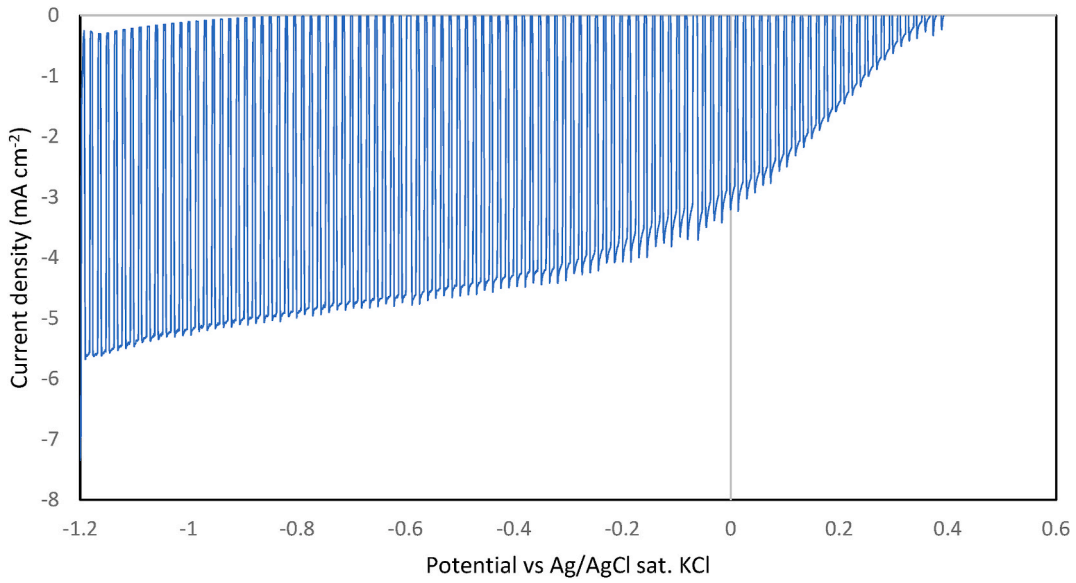

Fig. 4. Low scan linear sweep voltammetry (LSLV) curve of the Cu_2O photocathode in 0.1 M phosphate buffer solution at pH 7, exposed to one-sun light irradiation, T = 25 °C.

one expected from the transformed lactate to acetate (Eq. (3)), Q_{Acet} and lactate to bicarbonate (Eq. (4)), Q_{Bicar} using the Faraday's law after a given time t of electrolysis (Eqs. (10) and (11)):

$$ACE_{prod}^{Lact} = \frac{\int_0^t I\,dt}{Q_{Acet} + Q_{Bicar}} \tag{10}$$

where:

$$Q_{Acet} = 4 \cdot F \cdot S \cdot n_{\mathrm{Lact}}^{cons}$$

$$Q_{Bicar} = 12 \cdot F \cdot (1 - S) \cdot n_{\mathrm{Lact}}^{cons}$$

Where : n_{Lact}^{cons} is the amount of consumed lactate and F is the Faraday constant (96485 C mol^{-1} of electrons). Therefore,

$$ACE_{prod}^{Lact} = \frac{\int_0^t I\,dt}{4 \cdot F \cdot S \cdot n_{Lact}^{cons} + 12 \cdot F \cdot (1 - S) \cdot n_{Lact}^{cons}} \tag{11}$$

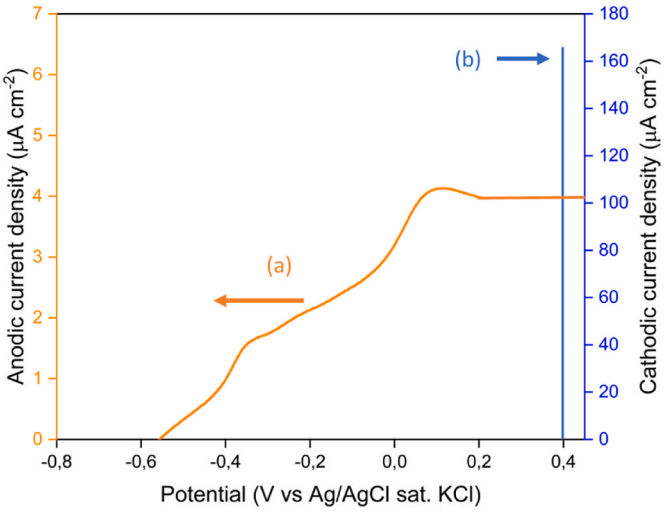

Fig. 5. Low scan linear sweep voltammetry (LSLV) curves. Scan rate 2 mV/s, T = 25 °C. (a) Bioanode: Electrolyte: 30 mM of lactate in minimal medium, OD_{600}: 0.234. (b) Photocathode: in 0.1 M phosphate buffer solution at pH 7, exposed to one-sun light irradiation.

2.8.3. Overall coulombic efficiency

The overall coulombic efficiency (anodic + cathodic) for the conversion of lactate to hydrogen ($OCE_{H_2}^{Lact}$) is the ratio between the experimentally measured quantity of hydrogen ($n_{H_2}^{exp}$) and the expected theoretical amount from the converted lactate ($n_{H_2}^{Lact}$) after a given electrolysis time t (Eq. (12)).

$$OCE_{H_2}^{Lact} = \frac{n_{H_2}^{exp}}{n_{H_2}^{Lact}} \tag{12}$$

Considering Eq. (3), Eq. (4) and the selectivity S (Eq. (7)), the theoretical amount of expected hydrogen from the converted lactate ($n_{H_2}^{Lact}$) can be calculated (Eq. (13)):

$$n_{H_2}^{Lact} = 2 \cdot S \cdot n_{Lact}^{cons} + 6 \cdot (1 - S) \cdot n_{Lact}^{cons} \tag{13}$$

from Eq. (12) and Eq. (13) the overall coulombic efficiency can be obtained (Eq. (14))

$$OCE_{H_2}^{Lact} = \frac{n_{H_2}^{exp}}{2 \cdot S\, n_{Lact}^{cons} + 6 \cdot (1 - S) \cdot n_{Lact}^{cons}} \tag{14}$$

It is worth noting that the three mentioned coulombic efficiencies (cathodic, anodic and global) are related (Eq. (15)):

$$OCE_{H_2}^{Lact} = ACE_{prod}^{Lact} \cdot CCE_{H_2}^{Q} \tag{15}$$

The above definitions consider that the intermediate oxidation product, acetate, can be further oxidized to bicarbonate and participate in current production (Eq. (16)).

$$CH_3COO^- + 4H_2O \rightarrow 2HCO_3^- + 9H^+ + 8e^- \tag{16}$$

Considering that acetate is electrochemically inactive toward further oxidation at the *Shewanella* biofilm and the final oxidation product of lactate oxidation at the bioanode is acetate (Eq. (3)), the anodic coulombic efficiency of lactate to acetate conversion $\left(ACE_{Acet}^{Lact}\right)$ and the overall coulombic efficiency $\left(OCE_{H_2}^{Lact/Acet}\right)$ can be calculated using Eq. (17) and Eq. (18), respectively.

$$ACE_{Acet}^{Lact} = \frac{\int_0^t I\,dt}{4 \cdot F \cdot n_{Lact}^{cons}} \tag{17}$$

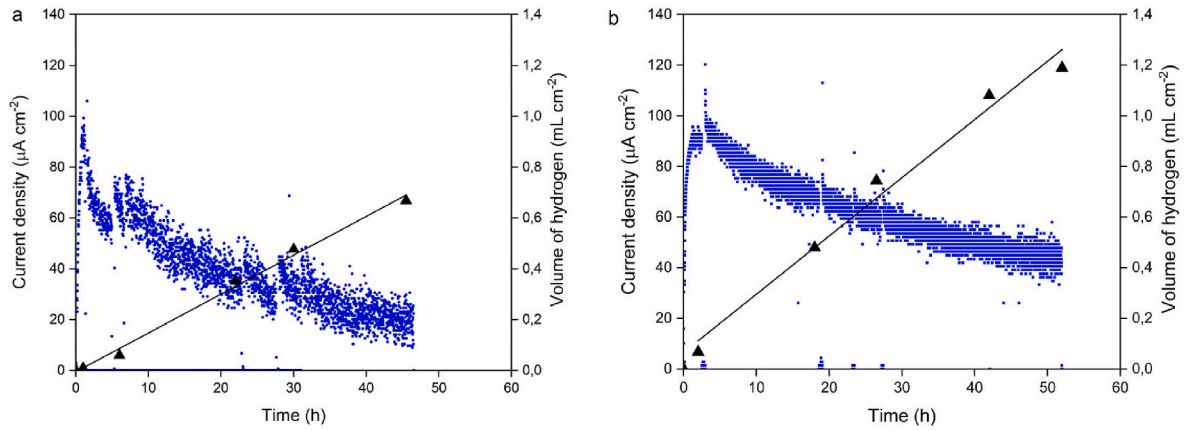

Fig. 6. Temporal evolution of the current density (with respect to the surface of the cathode) (■) and the specific volume of produced hydrogen (▲) at the photocathode under two simulated solar irradiations. (a) 210 W m^{-2} and (b) 700 W m^{-2}. Anolyte: medium (Section 2.3) with 20 mM of lactate. Catholyte: phosphate buffer 0.1 M pH 7, T = 25 °C, $S_{cathode}$ = 0.5 cm^2.

$$OCE_{H_2}^{Lact/Acet} = \frac{n_{H_2}^{exp}}{2 \cdot n_{Lact}^{cons}} \quad (18)$$

These equations are derived from Eqs. (11) and (14), respectively, by inserting $S = 1$.

3. Results and discussion

3.1. Electrochemical measurements

The photocurrent of the Cu_2O-based photocathode when exposed to one-sun light irradiation in 0.1 M phosphate buffer solution at pH 7, obtained by low-scan linear sweep voltammetry (LSLV) under intermittent illumination, is shown in Fig. 4. The cathodic photocurrent onset potential (100 μA cm^{-2}) is 0.37 V vs Ag/AgCl. The magnitude of the photocurrent increased sharply until −0.41 V vs Ag/AgCl, then increased linearly between −0.41 V and −1.2 V vs Ag/AgCl.

3.2. Current-potential curves of the bioanode and photocathode

The LSLV curve for an acclimatized *S. oneidensis* bioanode using MM as electrolyte is shown in Fig. 5a. The LSLV curve exhibited two distinct redox systems. The apparent half-wave redox potentials of these redox systems were −0.1 V vs Ag/AgCl (system I) and −0.39 V vs Ag/AgCl (system II). These redox systems have already been reported in the literature [33]. System I involved direct electron transfer (DET) where *S. oneidensis* was in direct contact with the anode and electrons are transferred from the outer membrane cytochromes of the bacteria to the anode surface. System II was related to the mediated electron transfer (MET) mechanism in which endogenous mediators, such as riboflavin and flavin mononucleotide (FMN) served as electron shuttles in the enzymatic oxidation of lactate.

The LSLV curve of the photocathode at the onset potential (0.37 ± 0.02 V) is reported in Fig. 5b. The two electrodes (bio and photo) are electrically connected in series. The current of the bio-photo electrochemical device is limited by the electrode that produces the lower current. The bioanode limits the current, as shown in Fig. 5, and its value is dependent on the maximum current of the anodic reaction. The anodic and cathodic current densities of the bio-photoelectrochemical device during electrolysis for hydrogen production (as shown in Section 3.3) can be estimated by overlapping the LSLV curves of both electrodes (bio and photo). Based in the values presented in Fig. 5, the anodic current density is 4.5 μA cm^{-2} and the cathodic current density is −100 μA cm^{-2}.

Table 2
Influence of light intensity on hydrogen production at the photocathode. The total electrical charge passed (Q_{tot}), hydrogen produced experimentally ($n_{H_2}^{exp}$); theoretical amount of produced hydrogen ($n_{H_2}^{theor}$), Eq. (9); cathodic coulombic efficiency ($CCE_{H_2}^{Q}$), Eq. (10). Conditions as in Fig. 6.

Irradiation (W m^{-2})	Q_{tot} (mC)	$n_{H_2}^{theor}$ (mmol)	$n_{H_2}^{exp}$ (mmol)	$CCE_{H_2}^{Q}$ (%)
210	4053	0.021	0.018	86
700	7527	0.039	0.033	85

3.3. Microbial-photo-electrochemical hydrogen production and influence of light

To determine the coulombic efficiencies involved in hydrogen production (anodic, cathodic and global), the microbial photo-electrochemical cell (MPEC, described in Section 2.3) with a Cu_2O-based semiconductor photocathode was exposed to light radiation and a *S. oneidensis* MR-1 pre-inoculated into the RVC bioanode (as described in Section 2.3) without any bias application has been used. The experiments were conducted at constant temperature of 25 °C.

The impact of light irradiance on the cathodic coulombic efficiency of hydrogen production ($CCE_{H_2}^{Q}$) was examined at two different light irradiation levels (210 W m^{-2} and 700 W m^{-2}). Fig. 6 shows the temporal progression of the cathodic current density and the specific volume of hydrogen production (mL of H_2 per unit cathode surface area) at the photocathode under both light irradiation levels at T = 25 °C. Fig. 6 illustrates that the initial cathodic current densities (100 μA cm^{-2}) for both light irradiation conditions are similar to the predicted values obtained from the interception of the LSLV curves of the bioanode and photocathode (Fig. 5).

Fig. 6 illustrates that the current density decreases over time and the specific production of hydrogen increases linearly during irradiation, under both light intensities. However, two differences were identified: a faster decrease in current at the lower intensity and a higher rate of specific volume of hydrogen produced at the higher intensity (700 W m^{-2}).

Table 2 shows the total electrical charge passed (Q_{tot}), the total amount of hydrogen produced $\left(n_{H_2}^{exp}\right)$, the expected theoretical amount of hydrogen produced $\left(n_{H_2}^{theor}\right)$, calculated using Eq. (9), and the cathodic coulombic efficiency $\left(CCE_{H_2}^{Q}\right)$, calculated from Eq. (8), for both irradiations.

Table 2 shows that, despite the higher irradiation (700 W m^{-2}) producing more hydrogen, both irradiations achieve similar current

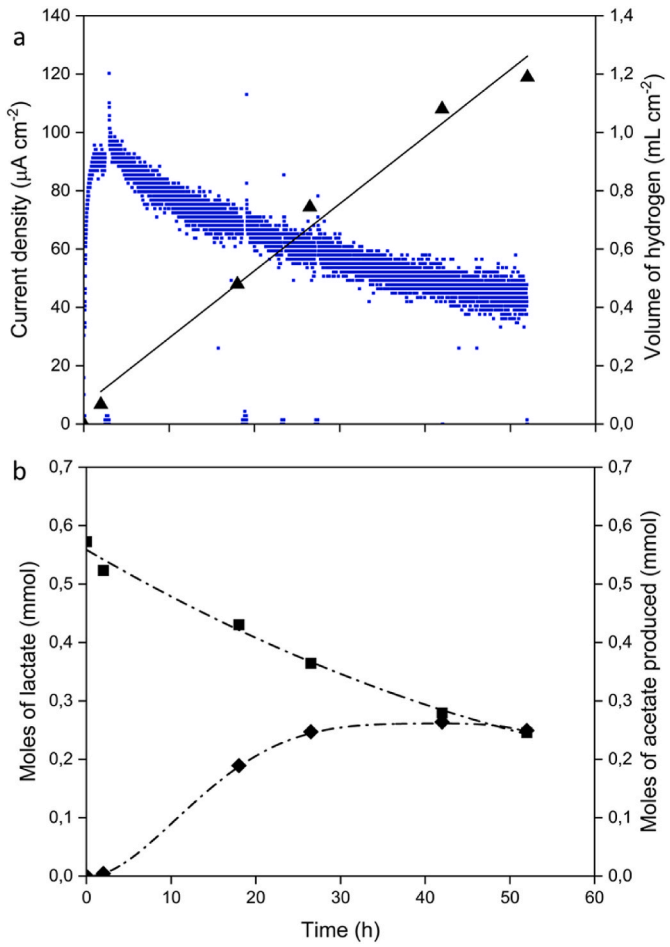

Fig. 7. (a) Temporal evolution of the current density (■) (with respect to the surface of the cathode) and hydrogen (▲) production during simulated solar illumination with a *S. oneidensis* MR-1 biofilm in MPEC at 700 W m^{-2}. (b) Lactate in the anolyte (■), acetate produced (◆). Conditions as in Fig. 6.

efficiencies (~85.5%). Two primary processes can result in cathodic efficiency losses during hydrogen production: faradaic and non-faradaic losses. Faradaic losses mainly occur due to the side reaction of dissolved oxygen reduction, resulting in the formation of H_2O_2 and/or H_2O, as represented by Eq. (19) and Eq. (20).

$$O_2 + 2H^+ + 2e^- \rightarrow H_2O_2 \quad (19)$$

$$O_2 + 4H^+ + 4e^- \rightarrow 2H_2O \quad (20)$$

Due to the relatively high solubility of oxygen in the catholyte, which is in equilibrium with air at 25 °C (0.2 mM), the occurrence of this side reaction is inevitable in the unaerated catholyte. Additionally, there are non-faradaic losses resulting from hydrogen gas leakage from the cell and the diffusion of dissolved hydrogen from the catholyte to the anolyte through the Nafion® membrane.

Table 4
Shewanella growth, using lactate as electron donor, under microaerobic conditions. Selectivity of lactate to acetate conversion as a function of lactate conversion (obtained from data in the literature [36]).

Lactate conversion %	20	40	55	88	100
$S_{Lact\ to\ Acet}$	0.29	0.21	0.36	0.06	0.13

3.4. Anodic and global coulombic efficiencies for H_2 production

A subsequent experiment was conducted under similar conditions to those in the previous series. However, it employed a solar irradiation of 700 W m^{-2} and monitored the composition of the reactant (lactate) and product (acetate) in the anolyte during electrolysis using HPLC.

Fig. 7 shows the evolution of current density, hydrogen production (Fig. 7a), mmol of unreacted lactate in the anolyte, and mmol of formed acetate (Fig. 7b).

Fig. 7b shows that the initial formation of acetate formed at first increased before reaching a plateau, in contrast to lactate which continued to be consumed. Table 3 presents the results obtained during the initial phase (t = 17 h) and at the end of the experiment (t = 52 h).

In this table, the amount of produced hydrogen ($n_{H_2}^{exp}$), unreacted moles of lactate (n_{Lact}^{cons}), and the formed acetate $\left(n_{Acet}^{form}\right)$ have been estimated, from Fig. 7. The theoretical amount of produced hydrogen $\left(n_{H_2}^{theor}\right)$ was determined using Eq. (9) along with the cathodic coulombic efficiency for hydrogen production $\left(CCE_{H_2}^{Q}\right)$ calculated using Eq. (8). The selectivity of lactate to acetate conversion (S) was determined by Eq. (7), Eq. (11) was used to calculate the anodic coulombic efficiency $\left(ACE_{\text{prod.}}^{Lact}\right)$ and Eq. (14) was used to calculate the overall coulombic efficiency $\left(OCE_{H_2}^{Lact}\right)$.

Table 3 indicates that the bioanode operation posed the primary limitation of the microbial photoelectrochemical system. Specifically, the anodic coulombic efficiency was much lower (3.8–9%) than the cathodic coulombic efficiency (85%), resulting in an a very low overall coulombic efficiency (5 ± 2%). Additionally, during the initial period of electrolysis (18 h), the selectivity of lactate to acetate transformation was equal to 1 ($S = 1$ in Eq. (7)), but the anodic coulombic efficiency remains low (~9%). Only 9% of the lactate transformed to acetate uses the anode as an electron acceptor, while the remaining 91% uses other soluble acceptors. Two potential electron acceptors are considered: protons and dissolved oxygen in the anolyte. Protons can participate in the fermentation of lactate to acetate and hydrogen (Eq. (5)) [29], while dissolved oxygen can be involved in the aerobic respiration of lactate to acetate and bicarbonate (Eq. (21)) [35].

$$C_3H_5O_3^- + 2\,H_2O \rightarrow CH_3COO^- + HCO_3^- + 5\,H^+ + 4e^- \quad (21)$$

However, the aerobic respiration of lactate to acetate is not complete even at low conversions (Table 4). This suggests that oxygen cannot be the electron acceptor during the initial stages of electrolysis (t = 17 h in Fig. 7b). The only possible explanation is the fermentation of lactate to acetate with hydrogen production in the anodic compartment (Eq. (5)).

During the late electrolysis period (t > 30 h in Fig. 7b), the reaction

Table 3
Obtained values after 17 and 52 h of electrolysis of the microbial photoelectrochemical cell (Fig. 7). Experimentally produced hydrogen ($n_{H_2}^{exp}$), theoretical amount of produced hydrogen ($n_{H_2}^{theor}$), cathodic coulombic efficiency for hydrogen production ($CCE_{H_2}^{Q}$), consumed lactate (n_{Lact}^{cons}), formed acetate (n_{Acet}^{form}), selectivity of lactate to acetate transformation (S), anodic coulombic efficiency $\left(ACE_{prod.}^{Lact}\right)$ and the overall coulombic efficiency $\left(OCE_{H_2}^{Lact}\right)$.

Time h	$n_{H_2}^{exp}$ mmol	$n_{H_2}^{theor}$ mmol	$CCE_{H_2}^{Q}$ %	n_{Lact}^{cons} mmol	n_{Acet}^{form} mmol	S (–)	$ACE_{\text{prod.}}^{Lact}$ %	$OCE_{H_2}^{Lact}$ %
17	0.010	0.012	85	0.19	0.19	1.0	9	7
52	0.033	0.039	85	0.35	0.27	0.77	3.8	3.2

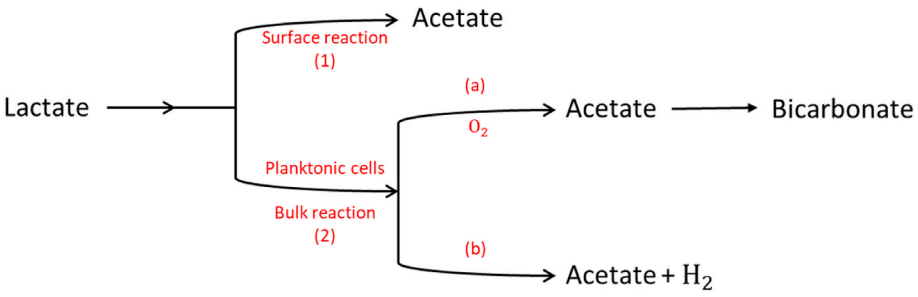

Fig. 8. Schematic representation of the proposed model, where parallel reactions take place: surface and bulk reactions. In the surface reaction lactate is oxidized at the bioanode to acetate, leading to current production. In the bulk reactions and in the presence of planktonic cells, lactate can be (a) aerobically oxidized to acetate and bicarbonate or (b) fermented to acetate and hydrogen, without current generation.

selectivity decreased ($S = 0.77$) and the amount of acetate remained constant. This indicates that all of the lactate that reacted during this period was converted into bicarbonate. Additionally, the anodic coulombic efficiency remained low (3.8%). This suggests that during the late electrolysis period, more than 96% of the reacted lactate did not contribute to the production of current. During the late electrolysis period, the main side reaction is the aerobic respiration of lactate in the bulk of the electrolyte, which is catalysed by planktonic cells (Eq. (22)).

$$C_3H_5O_3^- + 3\ O_2 \rightarrow 3HCO_3^- + 2H^+ \quad (22)$$

It is important to note that, despite the efforts to eliminate dissolved oxygen in the anolyte during our experiments, it was not feasible to sustain strictly anaerobic conditions due to the limitations of the used setup. Comparable challenges have been reported by other researchers [31]. Based on these considerations, a new model was proposed (Fig. 8) to explain the obtained low anodic coulombic efficiency. This model suggests that lactate may be involved in either a surface reaction at the bioanode (the main reaction producing current) or a bulk reaction catalysed by planktonic cells (a side reaction that consumes lactate without producing current).

At the bioanode, lactate is oxidized to acetate in the surface reaction (Eq. (3)), releasing 4 mol of electrons per mole of oxidized lactate (Eq. (3)) and producing electrical current (1 in Fig. 8). The kinetics of this reaction depend on the biocatalytic activity of the involved bacteria (*S. oneidensis* MR-1) and the thickness of the biofilm at the anode surface.

The oxidation of lactate in the bulk reaction is dependent on the type of soluble electron acceptor present in the anolyte. In the absence of oxygen (case b in Fig. 8), protons (water) act as electron acceptors, leading to the consumption of lactate and the production of acetate and hydrogen in the anolyte (Eq. (5)). If oxygen is present in the anolyte (case a in Fig. 8), lactate is oxidized to bicarbonate in an aerobic respiration process (Eq. (22)). These bulk reactions (a and b in Fig. 8) do not contribute to current production.

4. Conclusions

The study of the impact of light intensity on hydrogen production rate demonstrated that it was hindered by both the bioanode and the cathode, despite the bioanode having a larger surface area (12 cm^2) than the cathode surface area (0.5 cm^2).

The cathodic coulombic efficiency losses, which account for approximately 15%, are not affected by the value of the light intensity used (ranging from 210 to 700 W m^{-2}). The losses are expected to be mainly caused by side reactions related to the reduction of dissolved oxygen in the catholyte.

The low overall coulombic efficiency of lactate to hydrogen conversion, which is approximately 3%, is predominantly due to the anodic coulombic efficiency, which is only around 4%.

A model was proposed to explain the low anodic coulombic efficiency (Fig. 8). Under anaerobic conditions (absence of dissolved oxygen), protons (water) act as electron acceptors, leading to the consumption of lactate into acetate and hydrogen. On the other hand, under aerobic conditions (presence of dissolved oxygen), oxygen acts as an electron acceptor, leading to the complete oxidation of lactate to bicarbonate.

However, to confirm the validity of this model, measurements of hydrogen formed at the anode and the concentration of dissolved oxygen in the anolyte are necessary.

The average specific rates of hydrogen production achieved in this work were 15.4 μL h^{-1} cm^{-2} (210 W m^{-2}) and 26.1 μL h^{-1} cm^{-2} (700 W m^{-2}) based on the photoelectrode's surface. The latter value was at least 2.4 times greater than the most recent study result of 10.7 μL h^{-1} cm^{-2} with a bioanode [21] which employed an inoculum derived from the anaerobic sludge present in a wastewater treatment plant (WWTP).

CRediT authorship contribution statement

Michele Morgante: Formal analysis, Investigation, Visualization, Writing – original draft, Writing – review & editing, Methodology. **Nick Vlachopoulos:** Methodology. **Linfeng Pan:** Investigation. **Meng Xia:** Investigation. **Christos Comninellis:** Methodology, Writing – review & editing. **Kevin Sivula:** Investigation. **Michael Graetzel:** Writing – review & editing, Supervision. **Fabian Fischer:** Conceptualization, Funding acquisition, Methodology, Project administration, Supervision, Writing – review & editing.

Declaration of generative AI and AI-assisted technologies in the writing process

During the preparation of this work the authors used "DeepL write" to improve grammar, punctuation and style. After using this tool/service, the authors reviewed and edited the content as needed and take full responsibility for the content of the publication.

Declaration of competing interest

The authors declare that they have no known competing financial interests or personal relationships that could have appeared to influence the work reported in this paper.

Acknowledgements

The work was financially supported by the Swiss Federal Office of Energy, Project SI/501847, and from HES-SO Valais, University of Applied Sciences Western Switzerland as well as by EPFL. We thank Prof. Anders Hagfeldt for discussions on photocathode properties and their use. Michele Morgante worked full-time at HESSO Valais while enrolled at the EPFL doctoral school.

References

[1] United Nations. State of world population 2023. https://www.unfpa.org/sites/default/files/swop23/SWOP2023-ENGLISH-230329-web.pdf. [Accessed 16 August 2024].

[2] Murphy R. What is undermining climate change mitigation? How fossil-fuelled practices challenge low-carbon transitions. Energy Res Social Sci 2024;108:103390. https://doi.org/10.1016/j.erss.2023.103390.

[3] Batra V, Kaur I, Pathania D, Chaudhary V. Efficient dye degradation strategies using green synthesized ZnO-based nanoplatforms: a review. Appl Surf Sci Adv 2022;11:100314. https://doi.org/10.1016/j.apsadv.2022.100314.

[4] Emmanouilidou E, Mitkidou S, Agapiou A, Kokkinos NC. Solid waste biomass as a potential feedstock for producing sustainable aviation fuel: a systematic review. Renew Energy 2023;206:897–907. https://doi.org/10.1016/j.renene.2023.02.113.

[5] Call D, Logan BE. Hydrogen production in a single chamber microbial electrolysis cell lacking a membrane. Environ Sci Technol 2008;42:3401–6. https://doi.org/10.1021/es8001822.

[6] Blatter M, Furrer C, Cachelin CP, Fischer F. Phosphorus, chemical base and other renewables from wastewater with three 168-L microbial electrolysis cells and other unit operations. Chem Eng J 2020;390. https://doi.org/10.1016/j.cej.2020.124502.

[7] Saba SM, Müller M, Robinius M, Stolten D. The investment costs of electrolysis–A comparison of cost studies from the past 30 years. Int J Hydrogen Energy 2018;43(3):1209–23. https://doi.org/10.1016/j.ijhydene.2017.11.115.

[8] Mayyas A, Wei M, Levis G. Hydrogen as a long-term, large-scale energy storage solution when coupled with renewable energy sources or grids with dynamic electricity pricing schemes. Int J Hydrogen Energy 2020;45:16311–25. https://doi.org/10.1016/j.ijhydene.2020.04.163.

[9] Dincer I, Acar C. Review and evaluation of hydrogen production methods for better sustainability. Int J Hydrogen Energy 2014;40:11094–111. https://doi.org/10.1016/j.ijhydene.2014.12.035.

[10] Acar C, Dincer I. Review and evaluation of hydrogen production options for better environment. J Clean Prod 2019;218:835–49. https://doi.org/10.1016/j.jclepro.2019.02.046.

[11] Hosseini SE, Wahid MA. Hydrogen from solar energy, a clean energy carrier from a sustainable source of energy. Int J Energy Res 2020;44:4110–31. https://doi.org/10.1002/er.4930.

[12] Fischer F, Merino N, Sugnaux M, Huguenin G, Nealson KH. Microbial community diversity changes during voltage reversal repair in a 12-unit microbial fuel cell. Chem Eng J 2022;446. https://doi.org/10.1016/j.cej.2022.137334.

[13] Call DF, Wagner RC, Logan BE. Hydrogen production by *Geobacter* species and a mixed consortium in a microbial electrolysis cell. Appl Environ Microbiol 2009;75:7579–87. https://doi.org/10.1128/AEM.01760-09.

[14] Guo K, Prévoteau A, Patil SA, Rabaey K. Engineering electrodes for microbial electrocatalysis. Curr Opin Biotechnol 2015;33:149–56. https://doi.org/10.1016/j.copbio.2015.02.014.

[15] Liu H, Hu H, Chignell J, Fan Y. Microbial electrolysis: novel technology for hydrogen production from biomass. Biofuels 2010;1:129–42. https://doi.org/10.4155/bfs.09.9.

[16] Chae KJ, Choi MJ, Kim KY, Ajayi FF, Chang IS, Kim IS. A solar-powered microbial electrolysis cell with a platinum catalyst-free cathode to produce hydrogen. Environ Sci Technol 2009;43:9525–30. https://doi.org/10.1021/es9022317.

[17] Fischer F. Photoelectrode, photovoltaic and photosynthetic microbial fuel cells. Renew Sustain Energy Rev 2018;90:16–27. https://doi.org/10.1016/j.rser.2018.03.053.

[18] Morgante M, Vlachopoulos N, Hagfeldt A, Fischer F. Microbial bioelectrochemical cells for hydrogen generation based on irradiated semiconductor photoelectrodes. J Phys Energy 2021;3. https://doi.org/10.1088/2515-7655/ac01bd.

[19] Liang D, Han G, Zhang Y, Rao S, Lu S, Wang H, Xiang Y. Efficient H_2 production in a microbial photoelectrochemical cell with a composite Cu_2O/NiO_x photocathode under visible light. Appl Energy 2016;168:544–9. https://doi.org/10.1016/j.apenergy.2016.01.118.

[20] Chen QY, Liu JS, Liu Y, Wang YH. Hydrogen production on TiO_2 nanorod arrays cathode coupling with bio-anode with additional electricity generation. J Power Sources 2013;238:345–9. https://doi.org/10.1016/j.jpowsour.2013.04.066.

[21] Tahir MB. Microbial photoelectrochemical cell for improved hydrogen evolution using nickel ferrite incorporated WO_3 under visible light irradiation. Int J Hydrogen Energy 2019;44:17316–22. https://doi.org/10.1016/j.ijhydene.2019.01.067.

[22] He YR, Yan FF, Yu HQ, Yuan SJ, Tong ZH, Sheng GP. Hydrogen production in a light-driven photoelectrochemical cell. Appl Energy 2014;113:164–8. https://doi.org/10.1016/j.apenergy.2013.07.020.

[23] Jeon Y, Kim S. Persistent hydrogen production by the photo-assisted microbial electrolysis cell using a p-type polyaniline nanofiber cathode. ChemSusChem 2016;9(23):3276–9. https://doi.org/10.1002/cssc.201600906.

[24] Song S, Huang L, Zhou P. Efficient H_2 production in a $ZnFe_2O_4/g\text{-}C_3N_4$ photocathode single-chamber microbial electrolysis cell. Appl Microbiol Biotechnol 2023;107(1):391–404. https://doi.org/10.1007/s00253-022-12293-3.

[25] Bagal IV, Chodankar NR, Hassan MA, Waseem A, Johar MA, Kim DH, Ryu SW. Cu_2O as an emerging photocathode for solar water splitting-A status review. Int J Hydrogen Energy 2019;44(39):21351–78. https://doi.org/10.1016/j.ijhydene.2019.06.184.

[26] Bagal IV, Chodankar NR, Hassan MA, Waseem A, Johar MA, Kim DH, Ryu SW. Cu_2O as an emerging photocathode for solar water splitting - a status review. Int J Hydrogen Energy 2019;44:21351–78. https://doi.org/10.1016/j.ijhydene.2019.06.184.

[27] Son MK. Key strategies on Cu_2O photocathodes toward practical photoelectrochemical water splitting. Nanomaterials 2023;13:1–23. https://doi.org/10.3390/nano13243142.

[28] Jeon Y, Kim JH, Koo K, Kim S. A photo-assisted microbial electrolysis cell for the exclusive biohydrogen production using a MoS_2-coated p-type copper oxide. J Power Sources 2018;373:79–84. https://doi.org/10.1016/j.jpowsour.2017.11.003.

[29] Meshulam-Simon G, Behrens S, Choo AD, Spormann AM. Hydrogen metabolism in *Shewanella oneidensis* MR-1. Appl Environ Microbiol 2007;73:1153–65. https://doi.org/10.1128/AEM.01588-06.

[30] Rosenbaum M, Cotta MA, Angenent LT. Aerated *Shewanella oneidensis* in continuously fed bioelectrochemical systems for power and hydrogen production. Biotechnol Bioeng 2010;105:880–8. https://doi.org/10.1002/bit.22621.

[31] Joshi K, Kane AL, Kotloski NJ, Gralnick JA, Bond DR. Preventing hydrogen disposal increases electrode utilization efficiency by *Shewanella oneidensis*. Front Energy Res 2019;7:1–10. https://doi.org/10.3389/fenrg.2019.00095.

[32] Pan L, Kim JH, Mayer MT, Son MK, Ummadisingu A, Lee JS, Hagfeldt A, Luo J, Grätzel M. Boosting the performance of Cu_2O photocathodes for unassisted solar water splitting devices. Nat Catal 2018;1:412–20. https://doi.org/10.1038/s41929-018-0077-6.

[33] Baron D, LaBelle E, Coursolle D, Gralnick JA, Bond DR. Electrochemical measurement of electron transfer kinetics by *Shewanella oneidensis* MR-1. J Biol Chem 2009;284:28865–73. https://doi.org/10.1074/jbc.M109.043455.

[34] Qian F, Wang G, Li Y. Solar-driven microbial photoelectrochemical cells with a nanowire photocathode. Nano Lett 2010;10:4686–91. https://doi.org/10.1021/nl102977n.

[35] Tang YJ, Meadows AL, Keasling JD. A kinetic model describing *Shewanella oneidensis* MR-1 growth, substrate consumption, and product secretion. Biotechnol Bioeng 2007;96:125–33. https://doi.org/10.1002/bit.21101.

[36] Roy JN, Luckarift HR, Lau C, Falase A, Garcia KE, Ista LK, Chellamuthu P, Ramasamy RP, Gadhamshetty V, Wanger G, Gorby YA, Nealson KH, Bretschger O, Johnson GR, Atanassov P. A study of the flavin response by *Shewanella* cultures in carbon-limited environments. RSC Adv 2012;2:10020–7. https://doi.org/10.1039/c2ra21727a.